JOURNAL OF PROPULSION AND POWER
Vol. 14, No. 4, July–August 1998

Investigation of a Solid Fuel Scramjet Combustor

Adela Ben-Yakar,* Benveniste Natan,† and Alon Gany‡
Technion—Israel Institute of Technology, Haifa 32000, Israel

The combustion of a solid fuel under supersonic crossflow conditions in a scramjet configuration has been studied experimentally. Self-ignition and sustained combustion of poly-methyl-methacrylate with no external aid (such as reactive gas injection or a pilot flame) were demonstrated in static tests simulating a flight Mach number of about 5 at high altitude. The appropriate inlet conditions, i.e., stagnation temperature and pressure in excess of 1200 K and 16 atm, respectively, were provided by a vitiated air heater. The diverging combustion chamber included a fore-end flame stabilization zone, whose flameholding limits were determined experimentally. Flow and combustion phenomena were studied both by pressure measurements along the fuel grain and by video recording, taking advantage of the fuel transparency. Comparison between theoretical results of a one-dimensional flow model with test data showed fair agreement, indicating the existence of a supersonic flow regime within the combustor. The video pictures provided temporal and spatial fuel regression rate data, using a computerized image analysis system.

Nomenclature

A = port cross-sectional area of fuel grain
C_f = skin friction coefficient
c_p = specific heat at constant pressure
d = fuel port diameter
dx = axial distance of differential control volume
F = thrust
f = fuel-to-air ratio
G = flow mass flux
L = length of fuel grain
M = Mach number
$\dot{m}$ = mass flow rate
P = pressure
P_a = ambient pressure
R = gas constant
$\dot{r}$ = fuel regression rate
T = temperature
t = time
u = axial component of velocity
x_d = axial distance in diverging section
α = fuel divergent angle
γ = specific heat ratio
$\eta_{\Delta T}$ = temperature rise combustion efficiency
ρ = density
τ_w = friction
ς = equivalence ratio

Subscripts
air = air
cyl = constant diameter cylindrical section
d = diverging section
e = combustor exit
f = fuel
fl = flameholding zone
in = combustor inlet
t = total (stagnation) property
th = theoretical

Received Nov. 9, 1995; revision received May 4, 1997; accepted for publication Nov. 10, 1997.

*Graduate Student, Faculty of Aerospace Engineering; currently at Department of Mechanical Engineering, Stanford University, Stanford, CA 94305-3030.

†Senior Lecturer, Faculty of Aerospace Engineering. E-mail: aerbeny@aerodyne.technion.ac.il. Senior Member AIAA.

‡Professor, Faculty of Aerospace Engineering. Associate Fellow AIAA.

Introduction

THE selection of an appropriate air-breathing engine type is greatly affected by the design flight speed. Regarding the energetic performance, the ramjet engine is superior to the turbojet engine for flight Mach numbers greater than 3. Nevertheless, the stagnation pressure losses associated with the deceleration of the airflow from supersonic to subsonic increase with increasing flight Mach number and may substantially reduce the operating cycle efficiency (reflected by the specific impulse). Thus, for hypersonic flights (starting at Mach 5–7), a supersonic combustion ramjet (scramjet) or its derivatives, where the flow remains supersonic throughout the engine, are considered. Such devices exhibit better energetic performance because of lower stagnation pressure losses. An evaluation of the specific impulse vs Mach number for different jet engines is presented in Fig. 1.[1,2] Other significant advantages of the supersonic combustion cycle are associated with the lower static temperatures that permit extraction of more energy from the burning fuel (lower dissociation losses), and the lower static pressures implying smaller construction stresses.

Because of the recent interest in hypersonic vehicles, investigation of scramjet engines has received a great deal of attention. The main scramjet engine characteristics have been presented comprehensively.[3–5] Almost all supersonic combustion research has focused on liquid and gaseous fuels, mainly hydrogen, which demonstrates high energy, fast chemical kinetics, and good cooling properties.

However, the use of a solid fuel can substantially decrease complexity and cost and, in general, increase the energy density of the system, playing the same role as in rockets and conventional ramjets. Hence, the solid fuel scramjet seems to be advantageous for certain missions. For instance, it may be considered for boosting payloads or cargo to very high speeds, even as a part of propulsion systems to achieve orbit, as well as for accelerating kinetic energy missiles or penetrators.

The solid fuel scramjet should extend the use of the solid fuel ramjet (SFRJ) to the hypersonic flight range. Illustrations of the conventional (subsonic combustion) SFRJ as well as the solid fuel scramjet are presented in Fig. 2.

The solid fuel scramjet exhibits certain inherent features and operating problems, which are in part common to, but may be more severe than those encountered in the conventional SFRJ.[6,7]

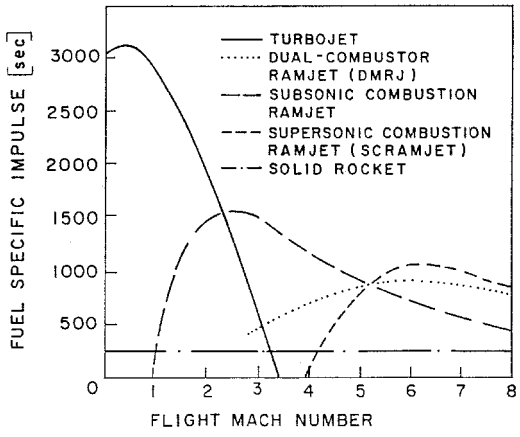

Fig. 1 Evaluation of specific impulse vs Mach number for different jet engines employing hydrocarbon fuel.[1,2]

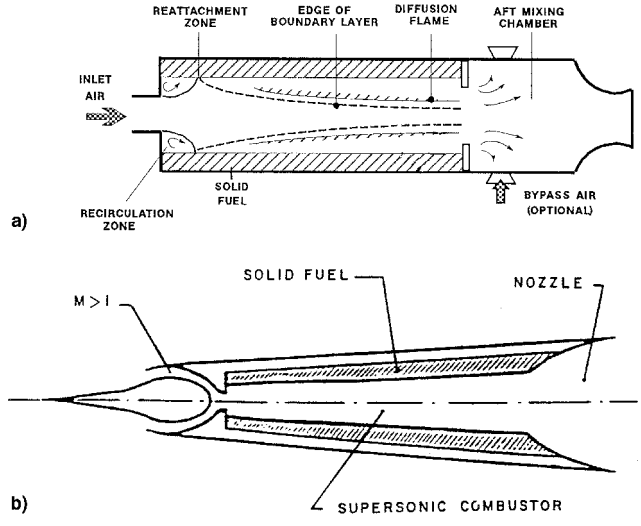

Fig. 2 Schematic diagrams of a) conventional (subsonic combustion) SFRJ and b) solid fuel scramjet.

1) In solid fuel scramjets as well as in SFRJs, the overall fuel-to-air ratio cannot be controlled directly because of the dependence of the fuel regression rate on the port flow characteristics (with major effects of G, T, and d).

2) The characteristic diffusion flame in SFRJs may result in a low combustion efficiency because of incomplete mixing of the fuel gases emerging from the wall and the oxygen diffusing from the core flow. The supersonic flow characteristics in the scramjet combustor further worsen the situation.

3) In contrast to hydrogen combustion, the combustion kinetics of the gasified hydrocarbon fuel may be slow compared to the residence time in the supersonic combustor (typically less than 1 ms).

4) Flameholding is a more difficult task in high-speed flows.

5) Internal port geometry should be designed carefully to avoid thermal choking and maintain supersonic flow throughout the operation.

Reports related to the solid fuel scramjet research are quite scarce in the literature. Vaught et al.[2] concluded that a solid fuel dual combustor ramjet consisting of a subsonic flow SFRJ-type combustor expelling its fuel-rich products into a supersonic flow combustor, may be a viable concept. In that study a four-step chemical kinetics scheme for hydrocarbon fuels[8] was used to demonstrate that the reaction can be completed in the supersonic combustor, once its initial slow steps take place within the subsonic combustor. Jarymowycz et al.[9] conducted a numerical study of the combustion of a solid fuel under supersonic crossflow. They concluded that combustion takes place in the gas phase above the fuel surface and that fuel regression rate is affected by the incoming air temperature and to a lesser extent by the pressure.

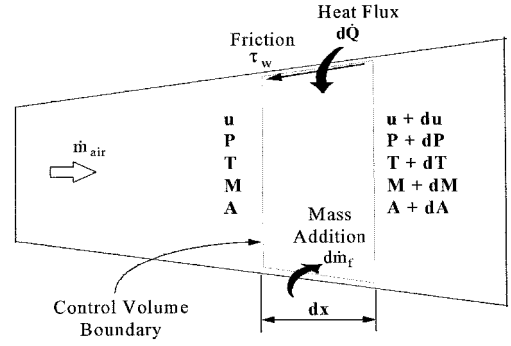

Fig. 3 Geometry and nomenclature for the differential control volume.

The only experimental work published to date on an SFRJ with supersonic combustion is the laboratory study by Angus et al.[10] The major significance of that study was the demonstration, in principle, of supersonic combustion (combustor exit Mach number as high as 1.4) of a solid fuel (Plexiglas®) at good combustion efficiencies. The combustor internal geometry was based on a flame stabilization zone that consisted of a sudden expansion of the inlet flow and a cavity in the fuel head end, as well as a diverging port combustor section in the downstream side. It was concluded that under the experimental operating conditions (inlet stagnation temperature of about 500 K), flame stabilization required the injection of a small amount of gaseous hydrogen. Nevertheless, according to the authors, good mixing was apparently achieved as a result of the surface roughness that is characteristic to the solid fuel scramjet.

The objective of the present research was to study the supersonic combustion of a solid fuel in a scramjet configuration. A dedicated connected-pipe static test facility was built to obtain experimental data on flameholding limits, fuel regression rate, and flow behavior. A one-dimensional flow analysis was used to compare the main theoretical and experimental trends.

Theoretical Analysis

A simplified, quasisteady one-dimensional theoretical analysis of the flow within the diverging section of the axisymmetric supersonic combustor was made to provide the basis for the initial combustor design and preliminary prediction of the flow behavior. The analysis takes into account mass addition because of the fuel gasification at the wall, heat addition because of combustion, and friction at the wall. Temporal and spatial variations of the port cross section because of the (nonuniform) wall regression are considered as well. No account is made for possible shock waves in the flow or for heat losses.

A perfect gas having uniform properties at each cross section at a given time is assumed. The relatively small temporal variations resulting from the fuel regression permit quasisteady treatment, where the entire flowfield is calculated for fixed dimensions at each time step.

The following are governing equations based on the conservation of mass, momentum, and energy in a differential control volume (Fig. 3) as well as on the perfect gas assumption:

$$\mathrm{d}(\rho u A) = \mathrm{d}\dot{m}_f \tag{1}$$

$$\mathrm{d}(\rho u^2 A) = -A\,\mathrm{d}P - C_{f\frac{1}{2}}\rho u^2 \pi d\,\mathrm{d}x \tag{2}$$

$$\mathrm{d}\left[\left(c_p T + \frac{u^2}{2}\right)\rho u A\right] = \mathrm{d}\dot{Q} \tag{3}$$

$$dP = d(\rho RT) \tag{4}$$

The differential form of Eqs. (1–4) is presented by a matrix in Eq. (5). The effects of variation of dimensionless cross section dA/A, fuel mass addition $d\dot{m}_f/\rho uA$, skin friction $2C_f\,dx/d$, and heat addition $d\dot{Q}/\rho uA \cdot u^2$ on the flow parameters u, T, M, and P can be derived from this matrix:

$$\begin{bmatrix} \frac{du}{u} \\ \frac{dT}{T} \\ \frac{dM^2}{M^2} \\ \frac{dP}{P} \end{bmatrix} = \begin{bmatrix} 1 & -1 & -\frac{(\gamma+1)M^2}{2(M^2-1)} & -1 \\ -(\gamma-1)M^2 & (\gamma-1)M^2 & \frac{(\gamma+1)M^2(\gamma M^2-1)}{2(M^2-1)} - (\gamma M^2+1) & (\gamma M^2-1) \\ 2+(\gamma-1)M^2 & -[2+(\gamma-1)M^2] & -\frac{[2+(\gamma-1)M^2](\gamma M^2+1)}{2(M^2-1)} & -(\gamma M^2+1) \\ -\gamma M^2 & 1+(\gamma-1)M^2 & \frac{[2+(\gamma-1)M^2]\gamma M^2}{2(M^2-1)} & \gamma M^2 \end{bmatrix} \begin{bmatrix} \frac{1}{M^2-1}\cdot\frac{dA}{A} \\ \frac{\gamma M^2}{M^2-1}\cdot 2C_f\frac{dx}{d} \\ \frac{d\dot{m}_f}{\rho uA} \\ \frac{(\gamma-1)M^2}{M^2-1}\cdot\frac{dQ}{\rho uA\cdot u^2} \end{bmatrix} \tag{5}$$

The fuel mass addition to the flow is calculated on the basis of measured values of the local regression rate, i.e.,

$$d\dot{m}_f = \rho_f \pi\, d\dot{r}\, dx \tag{6}$$

A reduced C_f value of 0.002 was assumed accounting for the wall blowing.[11]

The heat addition is a function of the fuel mass addition and the heat of reaction. It is obtained for each dx by assuming local chemical equilibrium and applying interactive calculation[12] of T_t and γ, accounting for the combustion efficiency i.e.,

$$d\dot{Q} = d(\dot{m}c_p T_t) \tag{7}$$

Experimental Apparatus and Procedure

Figure 4 shows a schematic diagram of the test facility and the data processing system. Air was provided from high-pressure tanks at typical mass flow rates of about 100–200 g/s (maximum capability 1 kg/s). Inlet stagnation temperatures and pressures as high as 1400 K and 20 atm, respectively, were obtained by passing the air through a vitiated air heater burning methane with oxygen makeup to maintain the oxygen mole fraction in the heater exhaust flow equal to that in air (0.21). Air, methane, and oxygen flows were regulated and measured using choked nozzles. The facility can simulate inlet stagnation conditions for flight Mach numbers greater than 5 at high altitude (10–15 km).

The supersonic combustor was made of transparent polymethyl-methacrylate (PMMA, Plexiglas), which also served as the solid fuel and permitted observation of the flow and combustion phenomena within its axisymmetric bore. The combustor shape crystallized from analysis and flameholding requirements of preliminary tests conducted in this facility, as well as from the experimental data of Ref. 10. The final combustor geometry (Fig. 5) consisted of an inlet (in), a flameholding zone (fh), which typically included a converging section (an oblique forward-facing step) at the downstream end of the flameholding zone, a constant diameter cylindrical section (cyl), and finally a long diverging section (d) to maintain supersonic flow with no choking.

A converging–diverging choked nozzle upstream of the combustor controlled the Mach number (1.6) at the combustor inlet and the stagnation pressure for a given flow rate. Monitoring and recording the combustion process using a super-VHS video cassette recorder (VCR) enabled on-line control of the experiments and posttest analysis of the video data.

Inlet air properties (total temperature and pressure) were measured in the plenum chamber before the converging–diverging nozzle at the combustor head end. The static wall pressure distribution along the combustor was obtained from pressure measurements through fine holes drilled in the fuel grain at six different axial locations (also shown in Fig. 5). The apparatus was mounted on a thrust stand to allow for continuous thrust measurement during firing.

The measured data such as pressure, temperature, gas flow rates, and thrust were gathered by a computerized data acquisition system using an analog to digital (A/D) board.

A computerized image processing system was used to obtain detailed information from the video recording. The system included a frame grabber, installed in one of the personal computer slots to transform the video images into digital signals (8-bit, 256 gray levels). A software package, CUE2, developed by Galai Production Ltd., Israel, was used to transfer these digital signals to the computer RAM. Storing the data on the computer hard disk was done prior to the image processing.

Post combustion analysis included transferring selected images from the VCR to the computer. The variation of the fuel port dimensions with time was obtained by direct measurement

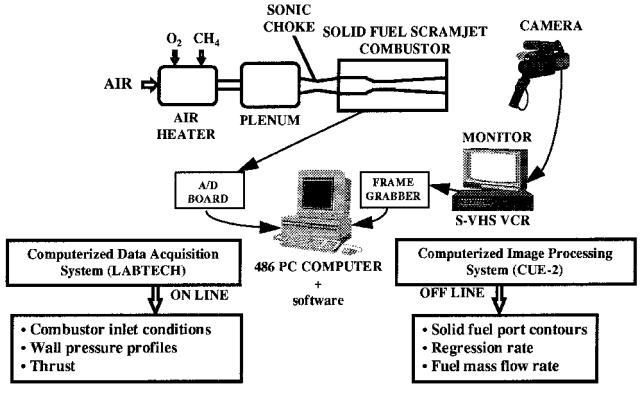

Fig. 4 Schematic of the experimental system including the data processing system.

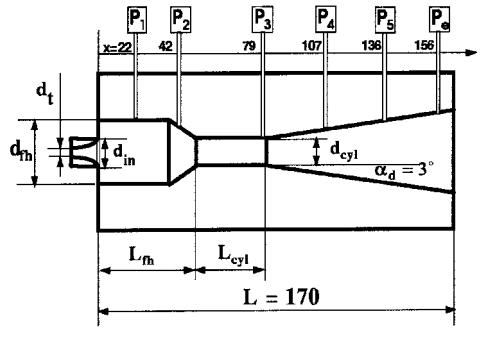

Fig. 5 Test combustor (dimensions in mm).

of the internal port contour from the video images at desired time intervals. The radial dimension of the field of view in the actual tests was 100–120 mm. Therefore, for a 512 × 512 pixel image, the resolution was about 0.2 mm per pixel. Having the internal port contour data, the temporal and spatial variations of the fuel regression rate were obtained. On this basis, the overall fuel mass flow rate vs time was calculated.

Results and Discussion

General

Operation of the test combustor was characterized by instantaneous self-ignition of the solid fuel by the incoming hot (1200 K) airflow. Neither igniter nor torch or other external means were used during the ignition or combustion stages. There was no preheating of the solid fuel.

Flameholding

Flameholding capability is essential for the operation of a solid fuel ramjet combustor and is practically accomplished by a sudden expansion of the incoming airflow using a rearward-facing step at the combustor inlet. The step acts as a bluff body, generating a recirculation zone characterized by relatively low velocities, high temperatures, and often high equivalence ratio. Analyses developed for premixed combustors[13,14] consider the recirculation zone essential for flame stabilization, serving as a continuous ignition source. Typically, flameholding models assume equality between characteristic residence and chemical reaction times (expressed by the so-called first Damkohler number), leading to a linear proportion of the blow-off velocity and the flameholder size for similar pressures and fuel:air ratios.[15] The fact that in SFRJs the recirculation zone length has been found linearly proportional to the step height[7,16,17] has resulted in a better flame-stabilizing effect for larger step heights. Netzer and Gany[7] noted that from the operational standpoint, smaller step heights are advantageous, as they allow more fuel to be placed in the combustor volume. Thus, one is interested in knowing the flameholding limits, namely, the minimum step height required for sustained combustion. Typically, flameholding limits for conventional (subsonic combustion) SFRJs have been presented in terms of the port-to-inlet area ratio (representing the step height) vs the port-to-exhaust nozzle throat area ratio (representing the flow velocity in the combustor).[7,17,18] This approach is, in essence, another way to represent the two main parameters used in flameholding analyses.

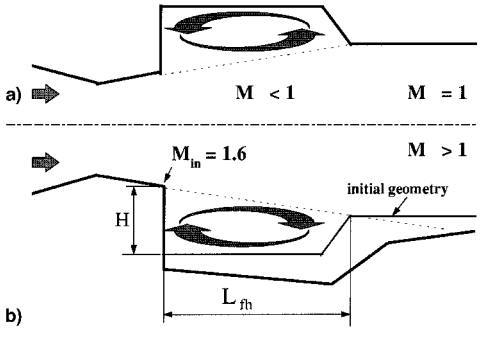

Fig. 6 Schematic of the flameholding section: a) initial stage (ignition) and b) after stage (combustion).

Because the internal flow velocities associated with scramjet operations are much higher than those of subsonic combustors, flameholding in the supersonic combustion SFRJ is expected to be much more difficult, requiring larger step heights. The common sudden expansion configuration may thus be impractical in such a case for two main reasons:

1) A larger inlet step would further decrease the actual fuel amount in a given combustor volume.

2) Because of the supersonic flow regime, the resulting larger port cross section would further increase the freestream flow velocity, deteriorating the flameholding capability.

Recognizing these special conditions, a modified flame stabilization zone has been applied, consisting of a constant cross-sectional recess in the foremost part of the fuel bounded by an inlet rearward-facing step in the upstream direction and an incline forward-facing step in the downstream side. A recess is considered a possible alternative for flame stabilization. A similar arrangement was used in Ref. 10. Limited flame stabilization zones were also generated in this way within the combustor of the recently flight-tested (hydrogen-fueled) scramjet onboard the Hypersonic Flying Laboratory Kholod.[19]

Considering the physical aspects associated with the flameholding zone, a distinction should be made between the first few seconds of the motor operation (ignition) and the rest of the time (combustion). During ignition stage the flow is probably choked downstream the flameholding zone because of heat addition and the small initial diameter of the cylindrical section. Under these conditions, a shock wave occurs somewhere at the diverging section of the air inlet nozzle, resulting in subsonic conditions throughout the whole flameholding section (Fig. 6a). However, as the solid fuel surface regresses, the internal cross-sectional area grows and the flow ceases to be thermally choked, implying supersonic conditions in the core flow throughout the engine. Then, the flow consists of two main parts: 1) the freestream zone whose initial Mach number is supersonic (~1.6), and 2) the recirculation zone that is partially subsonic (Fig. 6b). Unlike the regular inlet geometry in subsonic flow SFRJ combustors, where the recirculation zone length is proportional to the step height, in the current supersonic combustor the recirculation zone size is determined by both the step height and the geometrical length L_{fh}.

The modified flameholding parameters chosen to represent the flameholding limits in the present configuration are $d_{fh}L_{fh}/d_{in}^2$, representing the relative size of the flameholding zone, and $(d_{fh}/d_{cyl})^2$ as a measure of the flow velocity.

Table 1 Summary of the flameholding section geometry parameters and test conditions

Test no.	$\dot{m}_{in}$, g/s	$P_{t,in}$ atm	$T_{t,in}$ K	d_{fh}, mm	d_{cyl}, mm	L_{fh}, mm	L_{cyl}, mm	Comments
1	182.4	15.66	1033	25	14.5	50	35	Sustained combustion
2	180.7	16.47	1168	25	14.5	50	15	Sustained combustion
3	184.2	16.72	1159	25	14.5	30	35	Extinguished after 2 s
4	183.6	16.28	1105	20	14.5	50	35	Extinguished after 2.5 s
5	**183.8**	**16.68**	**1156**	**30**	**14.5**	**50**	**35**	**Sustained combustion**
6	179.3	16.48	1183	35	14.5	50	35	Sustained combustion
7	170.7	15.83	1216	20	14.5	70	15	Extinguished after 5.5 s
8	177.2	——	——	30	20.1	50	55	Extinguished after 5.5 s
9	177.7	17.50	1378	30	16.5	50	35	Sustained combustion
10	180.1	18.00	1392	30	16.5	40	45	Sustained combustion
11	179.3	18.00	1410	20	11.5	50	35	Extinguished after 2 s
12	182.7	17.20	1241	30	14.5	50	35	Sustained combustion Metal disc at the rear end

Table 1 presents the operating conditions and combustor geometry in 12 firing tests aimed at determining the flameholding limits. Typically, the tests used an air inlet nozzle of d_t = 11.05 mm, and d_{in} = 12.45 mm, resulting in a Mach number of 1.6 at the end of the inlet. The α_d was 3 deg (Fig. 5). Most of the tests were operated with similar air properties (total pressure about 16 atm, total temperature about 1200 K) and flow rates (~180 g/s). Parameters applicable to the flameholding capability (d_{fh}, L_{fh}, d_{cyl}, L_{cyl}) were varied systematically.

Figure 7 presents the test data in terms of the modified flameholding parameters. The results reveal a limit between the sustained combustion tests (upper right-hand side of the graph) and the nonsustained combustion tests (below and to the left of the limit line).

As shown in Table 1 and Fig. 7, a flameholding section diameter d_{fh} as small as 20 mm (test no. 4), did not permit sustained combustion even for quite long L_{fh} (50 mm). In spite of self-ignition of the fuel, the combustion was self-extinguished 2.5 s after the ignition, as the gas flow velocity in the flameholding section increased because of the growing area of the downstream cylindrical section during burning. Too short a length of the flameholding section (L_{fh} = 30 mm) caused flameout as well, even for relatively large d_{fh} (25 mm, see test no. 3).

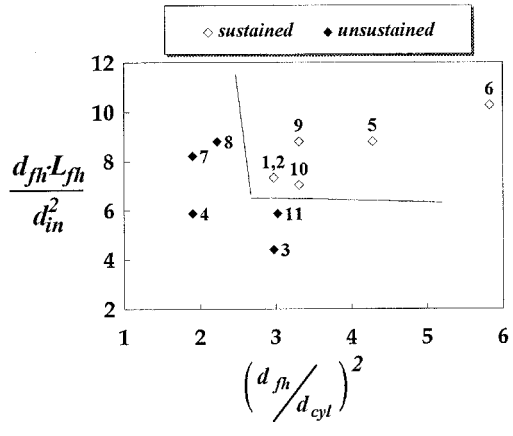

Fig. 7 Flameholding limits in the solid fuel scramjet combustor. The fuel is PMMA and the total air temperature is 1200 K (numbers near test points refer to Table 1).

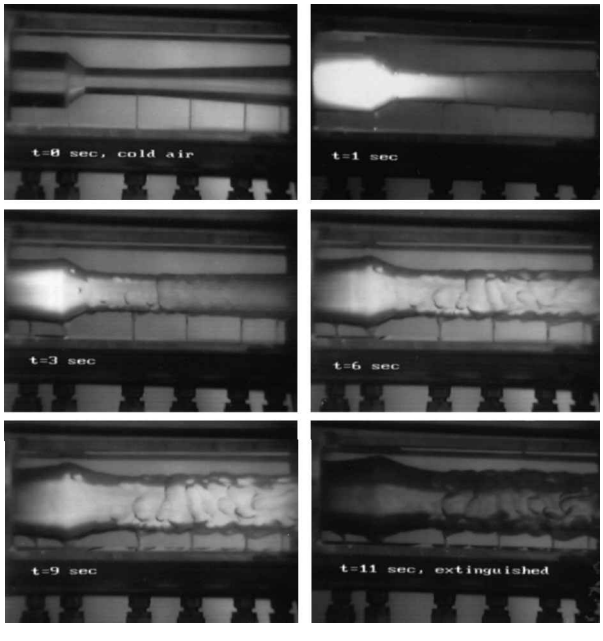

Fig. 8 Sequence of video images of fuel combustion.

Fuel Regression

The ability to acquire and digitally process video images of the combustion and burning surface of the transparent PMMA fuel, permitted continuous presentation of the flame development and internal port contour at high spatial and temporal resolution. Figure 8 presents a sequence of six video photographs of test no. 5, which lasted for 11 s. The images reveal that the flame spreads from the flameholding zone to the downstream diverging section. During burning, the internal cross-sectional area is growing continuously while the port divergence is decreasing. A characteristic surface waviness and roughness can be observed in the diverging section. This pattern, which has also been observed by Netzer et al.,[10] seems to be peculiar to combustion in supersonic flow, possibly a result of shock train—boundary-layer interactions.

Figure 9 presents the variations of the port contour with time corresponding to Fig. 8. The change of the local port radius with time provided the local fuel regression rate (Fig. 10). As can be seen, different zones exhibit different behavior and magnitude of regression rate. The initial flameholding zone is characterized by a relatively low regression rate. The sharp edge of the oblique step at the downstream end of the flameholding zone exhibits the peak regression rate. The cylindrical section downstream of the flameholding zone demonstrates a high regression rate during the initial stage, and an average value later on. The diverging section of the grain shows a monotonic decrease in regression rate with the axial location. Note that the fuel regression rate pattern varies with time, as the burning tends to flatten the port profile causing the bore to become more cylindrical and the local regression rate to be more uniform regarding the axial variation. This behavior is apparent from Fig. 9 and is emphasized in Fig. 10 which, in addition to the time-average local regression rate along the grain, shows the corresponding values for the first 5 and the last 6 s. As expected, the regression rate decreases with time because of the enlargement of the flow cross section.[20,21] The time dependence of the spatially mean regression rate is depicted in Fig. 11, revealing monotonic decrease with time.

Integrating the instantaneous local fuel regression rate over the burning surface yielded the instantaneous overall fuel mass

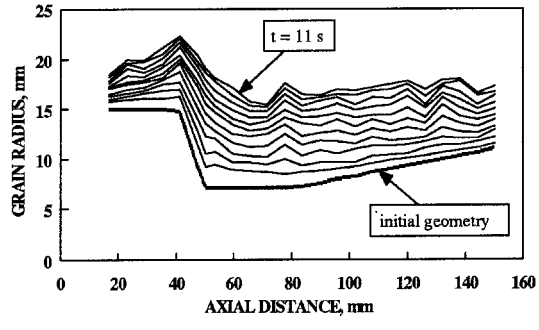

Fig. 9 Variation of the fuel port contours during burning at time intervals of 1 s. Test no. 5.

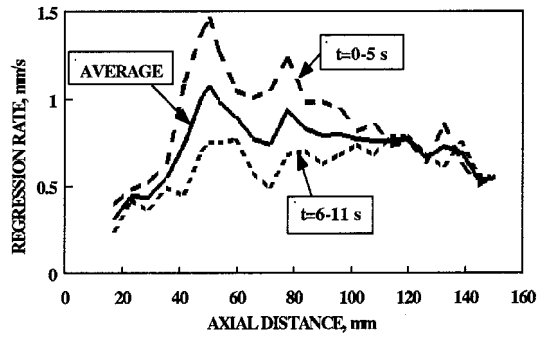

Fig. 10 Axial variation of the time-average local regression rate.

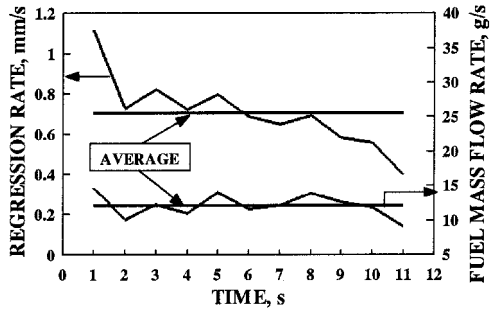

Fig. 11 Temporal dependence of the spatially mean regression rate and overall fuel mass flow rate.

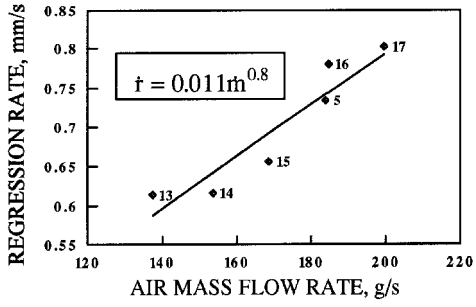

Fig. 12 Influence of the air mass flow rate on the average solid fuel regression rate.

flow rate [Eq. (6)], taking into account the PMMA fuel density (1.2 g/cm^3). The dependence of $\dot{m}_f$ on time is also shown in Fig. 11. It seems that $\dot{m}_f$ is almost constant throughout the burning time (12 ± 2 g/s) because of the opposing effects of the decreasing regression rate and increasing burning surface. Consequently, the overall f is also constant (0.065 ± 0.01) because the inlet airflow rate does not change (184 g/s). The corresponding equivalence ratio is thus $\varsigma = 0.5 \pm 0.1$ (the stoichiometric fuel:air ratio for PMMA is 0.121).

For the evaluation of the mass flow rate effect on the fuel regression rate, additional tests were conducted with the same geometry as test no. 5. In these tests the burning time (10 s) and the inlet total air temperature (~1200 K) were kept constant while the air mass flow rate was varied systematically over the 137–200 g/s range. The test results reveal a monotonic increase in the average regression rate when the increasing incoming airflow rate. For the specific geometry tested, the following correlation between the mean regression rate and mass flow rate was found:

$$\dot{r} = 0.011\dot{m}^{0.8} \tag{8}$$

where $\dot{r}$ is in (mm/s) and $\dot{m}$ is in (g/s) (Fig. 12). It is noteworthy that in spite of the nonuniformity of the port diameter and the totally different internal flow regime, both the power dependence (0.8) and the magnitude of the average regression rate range (~0.6–0.8 mm/s) are similar to the values obtained for subsonic SFRJ combustors with an average G of the same order (~20–25 g/cm^2-s),[6,15,21] indicating the dominant influence of convective heat transfer on the regression rate.

Internal Ballistics and Flow Characteristics

Detailed information about the flow behavior within the combustor was obtained by continuous wall pressure measurements at six different axial locations (Fig. 5). Figure 13 presents the six pressure traces vs time as obtained in a typical test (test no. 5 in Table 1). Operation starts with cold airflow through the combustor, causing a static pressure of 1.5–2.5 atm in the flameholding zone and cylindrical section, and a subatmospheric pressure in the diverging section. Ignition in the vitiated air heater implies immediate elevation of the flow stagnation temperature to its steady-state value (~1200 K), causing instant self-ignition of the solid fuel in the combustor. The flow is then characterized by relatively high pressure in the flameholding zone (about 8 atm, pressure transducers 1 and 2), somewhat lower, but still high pressure at the end of the cylindrical cross section (about 6 atm, transducer 3), and much lower pressures in the diverging section (1–2 atm, transducers 4, 5, exit). It is also obvious that the pressures indicated by the first three gauges decrease monotonically, attaining relatively low values (~2 atm) before burnout, while the gauges in the diverging section indicate more steady and slightly increasing pressures with time. Figure 14 uses the data of Fig. 13 to present the variation of pressure distribution along the combustor with time. The axial pressure distribution indicates that the flameholding zone and the cylindrical section are apparently choked, at least during the first few seconds of burning, until the cylindrical section opens up significantly. This interpretation can be supported by previous indications that the heat addition in the flameholding zone is likely to cause thermal choking. On the other hand, the behavior of the flow in the diverging section seems to exhibit supersonic characteristics. A combined experimental and analytical effort was made to support this hypothesis.

A one-dimensional analytical solution for the flow in the diverging section of the combustor during the first few seconds of burning was obtained. For the boundary conditions at the beginning of the diverging section a Mach number of unity and equilibrium temperature were assumed. The equilibrium temperature calculation was based on the ratio of the actual air mass flow rate to the actual fuel consumption rate accounting for the combustion efficiency in the flameholding section. The measured fuel regression rate along the grain (Fig. 10) was used as input data for the fuel mass addition. Heat addition

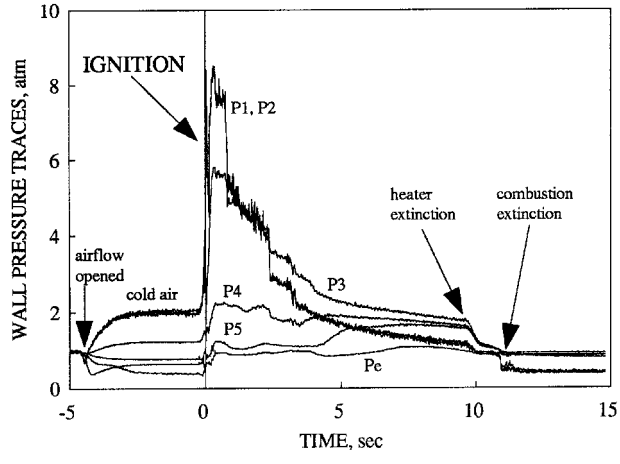

Fig. 13 Traces of pressure vs time as obtained from six pressure transducers located in different axial distances during a typical test (no. 5).

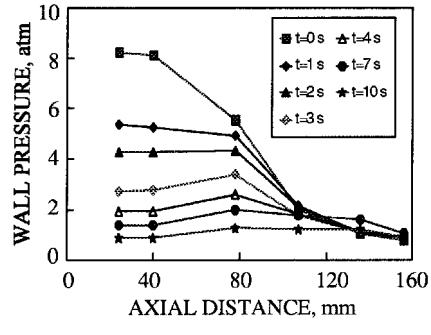

Fig. 14 Variation of pressure distribution along the combustor with time (t is measured from ignition).

calculations in the diverging section took into account the combustion efficiency obtained in the tests.

Figure 15 presents a comparison between the measured pressure along the diverging combustor section at different burning times (test no. 5, Table 1) and the calculated values obtained for a supersonic combusting flow. The regression rate in the diverging section and the combustion efficiency values used for this comparison were based on actual time-averaged (first 5 s) experimental results. It should be noted that the combustion efficiency had only a small effect on the calculation. The agreement of the calculated static pressure with the measured wall pressure is very good at the initial cross section and continues to be fairly good further downstream, particularly in the light of the idealized, one-dimensional shock-free calculation. The similar theoretical and experimental results indicate that the nature of the flow is supersonic. In the case of subsonic flow, the static pressure values should be considerably higher than those under supersonic flow regime for the same stagnation pressure conditions. In addition, the stagnation pressure losses because of heat addition are expected to be lower for subsonic freestream conditions.

Special experiments were designed to demonstrate in a more definite manner the supersonic combusting flow behavior compared to subsonic combustion characteristics. These experiments consisted of the same fuel grain configuration and the same operating conditions as in the previous tests. However, a metal disc having a concentric hole equal to the combustor exit diameter was attached to the rear end of the grain. During the initial combustion period the disc was expected to have no effect on the flow regime, permitting supersonic conditions to be established within the combustor. However, with the enlargement of the fuel port during combustion, the fixed internal diameter of the disc was expected to choke the flow, switching to subsonic regime.

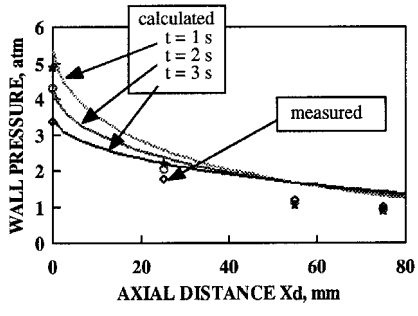

Fig. 15 Comparison between the wall pressure measurements along the diverging combustor section and supersonic combusting flow theoretical calculation.

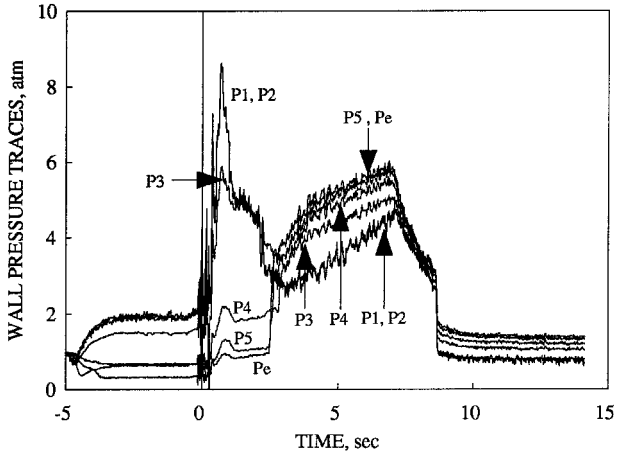

Fig. 16 Traces of pressure vs time at different axial locations in a test with an aft-disc.

Figure 16 shows the pressure vs time traces of a test (test no. 12 in Table 1), where a disc of a fixed internal diameter (23 mm) was placed in the rear end of the combustor. The fuel grain configuration and operating conditions were similar to those of test no. 5 (unchoked), whose data are given in Table 1 and test results are shown in Figs. 13 and 14.

During the first 2.2 s of burning the pressure traces in Fig. 16 reproduced those of Fig. 13, indicating the same flow regime where supersonic flow is very likely to have taken place in the diverging section (pressure transducers nos. 4, 5, e). An appreciable abrupt pressure increase was detected at the rear end (transducer *e*) after approximately 2.2 s and was further recorded by the transducers upstream of *e*-station in small time intervals. The pressure in the different stations remained high for the rest of the burning time exhibiting a gradual increase.

It is hypothesized that once choking conditions are established by the aft restricting disk, a strong shock front propagates upstream, generating a subsonic flow regime throughout the combustor to accommodate the back pressure. When subsonic regime is established the surface roughness disappears.

Table 2 presents the measured pressures (P, P' respectively) before and after the shock front and the corresponding Mach numbers (M, M'), assuming normal shock conditions with $\gamma = 1.28$. A comparison between the incident Mach numbers of Table 2 and the calculated values resulting from the one-dimensional supersonic flow computation for the diverging section is shown in Fig. 17. Note that x_d is the axial distance along the diverging section [$x_d = x - 85$ (mm)].

The interpretation of the results in terms of a normal shock establishment strongly supports the assumed supersonic combustion regime before the effect of the choking disc. The trend and magnitude of Mach number variation along the diverging combustor section are similar to the theoretical behavior. Initial choking conditions (at the aft-end) also agree with the disk and port flow area ratio. The increase of static pressure with time and axial distance, i.e., as a result of heat addition and port enlargement after the choking instant (Fig. 16), indicates the shift from supersonic to subsonic regime, and the totally different nature of the flow.

Thrust measurement enables the evaluation of additional operating parameters. The motor thrust is given by

$$F = \dot{m}u_e + (P_e - P_a)A_e \tag{9}$$

Using the continuity equation and assuming perfect gas behavior, the exit Mach number M_e is obtained and is described by

$$M_e = \left[\frac{F - (P_e - P_a)A_e}{\gamma_e P_e A_e}\right]^{1/2} \tag{10}$$

All of the parameters in Eq. (10) are measured in the test except γ_e, which is estimated as 1.28 based on thermochemical calculations. The estimated error in the value of M_e is relatively small ($\pm 2.5\%$). T_e and u_e are obtained by

$$\dot{m}_e = \rho_e u_e A_e = P_e M_e A_e \sqrt{\gamma_e / R_e T_e} \tag{11}$$

R_e is calculated from the gas composition assuming chemical equilibrium ($R_e = 0.29$ kJ/kg-K). Total temperature and pressure at the exit plane (T_{te} and P_{te}) are calculated from the static properties and Mach number. Finally, the combustion efficiency is calculated on the basis of the total temperature rise

$$\eta_{\Delta T} = \frac{T_{te} - T_{t,in}}{T_{te,th} - T_{t,in}} \tag{12}$$

Table 2 Measured pressures before and after the shock front and the corresponding normal shock Mach numbers

Station	t, s	x, mm	P, atm	P', atm	P'/P	Initially subsonic or sonic conditions M	M'
1	2.7	22	2.7	2.7	1.0	——	——
2	2.7	42	2.7	2.7	1.0	——	——
3	2.7	80	3.25	3.35	1.03	——	——
4	2.5	107	2.1	3.2	1.52	1.21	0.83
5	2.2	135	1.1	3.0	2.73	1.60	0.66
e	2.2	155	0.96	3.5	3.65	1.83	0.60

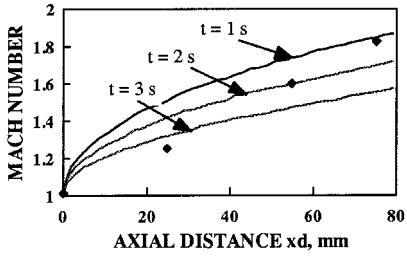

Fig. 17 Experimental Mach numbers along the diverging combustor section (as implied from measured pressure jump) compared to theoretical values.

The adiabatic flame temperature $T_{te,th}$ is determined utilizing the PEP thermochemical code.[12]

In a typical test, e.g., test 5 in Table 1, $P_a = 1$ atm, P_e stayed very close to 1 atm (within $\pm 4\%$), and the fuel:air ratio remained approximately constant (0.065 ± 0.005). Supersonic exit conditions were indicated throughout the test, in agreement with the theoretical predictions and previous experimental results. Of practical significance is the fact that a relatively slight variation in thrust level was exhibited during the operation time (from 23 to 20 kgf) in spite of the appreciable geometric variations (it did, however, exhibit high-frequency oscillations of ± 3 kgf).

In general, both static and stagnation temperatures seemed to increase monotonically with time, implying an increase in combustion efficiency from about a 40 to 50% level. Combustion efficiency was also found to increase monotonically when decreasing the airflow rate for the same fuel geometry. However, indirect experimental determination of T_{te} implies a large inaccuracy in the efficiency values, which may include a relative error in excess of $\pm 20\%$. The relatively low attainable combustion efficiency is attributed to the nonuniform flow properties at the exit cross section and to the small combustor size. A higher combustion efficiency could probably be obtained for a longer fuel grain and for optimized geometry and airflow rate.

Concluding Remarks

A solid fuel supersonic laboratory combustor has been analyzed, designed, and successfully demonstrated experimentally, simulating inlet conditions encountered at a flight Mach number of 5, i.e., total air temperature and pressure of 1200 K and 16 atm, respectively.

Self-ignition of a PMMA solid fuel by hot airflow was demonstrated.

A mixed supersonic subsonic flow recirculation zone was used for flameholding. Flameholding geometric conditions were investigated, and actual flameholding limits were presented experimentally.

Sustained combustion could be maintained in supersonic flow (for a Mach number as high as about 2). The existence of supersonic flow conditions was revealed in actual tests. A simplified shock-free analysis provided a fair description of the trends and magnitude of the supersonic flow parameters.

Fuel regression rate as well as combustor port are generally characterized by temporal and spatial variations. However, the overall fuel flow rate and fuel:air ratio as well as the engine thrust were found to be approximately constant throughout the burning. Also, the average regression rate showed a dependence on the airflow rate to the 0.8 power, indicating the role of forced convection.

Combustion efficiency was found to increase with time and when decreasing airflow rate. Higher efficiencies could be obtained by optimizing the combustor geometry and airflow rate.

References

[1]Billig, F. S., "Tactical Missile Design Concepts," *Johns Hopkins APL Technical Digest*, Vol. 4, No. 3, 1983, pp. 139–154.

[2]Vaught, C., Witt, M., Netzer, D. W., and Gany, A., "Investigation of Solid Fuel, Dual-Mode Combustion Ramjets," *Journal of Propulsion and Power*, Vol. 8, No. 5, 1992, pp. 1004–1011.

[3]Northam, G., and Anderson, G. Y., "Supersonic Combustion Ramjet Research at Langley," AIAA Paper 86-0159, Jan. 1986.

[4]Waltrup, P. J., "Liquid-Fueled Supersonic Combustion Ramjet: A Research Perspective," *Journal of Propulsion and Power*, Vol. 3, No. 6, 1987, pp. 515–524.

[5]Billig, F. S., "Research on Supersonic Combustion," *Journal of Propulsion and Power*, Vol. 9, No. 4, 1993, pp. 499–514.

[6]Zvuloni, R., Levy, Y., and Gany, A., "Investigation of a Small Solid Fuel Ramjet Combustor," *Journal of Propulsion and Power*, Vol. 5, No. 3, 1989, pp. 269–275.

[7]Netzer, A., and Gany, A., "Burning and Flameholding Characteristics of a Miniature Solid Fuel Ramjet Combustor," *Journal of Propulsion and Power*, Vol. 7, No. 3, 1991, pp. 357–363.

[8]Hautman, D. J., Dryer, F. L., Schung, K. P., and Glassman, I., "A Multiple-Step Overall Kinetic Mechanism for the Oxidation of Hydrocarbons," *Combustion Science and Technology*, Vol. 25, Nos. 5–6, 1981, pp. 219–235.

[9]Jarymowycz, T., Yang, V., and Kuo, K. K., "A Numerical Study of Solid Fuel Combustion Under Supersonic Crossflows," *Journal of Propulsion and Power*, Vol. 8, No. 2, 1992, pp. 346–353.

[10]Angus, W. J., Witt, M. A., Laredo, D., and Netzer, D. W., "Solid Fuel Supersonic Combustion," *La Recherch Aerospatiale*, No. 6, 1993, pp. 1–8.

[11]Marxman, G., "Combustion in the Turbulent Boundary Layer on a Vaporizing Surface," *10th Symposium (International) on Combustion*, The Combustion Inst., Pittsburgh, PA, 1965, pp. 1337–1349.

[12]Cruise, D. R., "Theoretical Computation of Equilibrium Composition, Thermodynamic Properties, and Performance Characteristics of Propellant Systems (PEP Code)," Naval Weapons Center, China Lake, CA, April 1979.

[13]Longwell, J. P., "Combustion Problems in the Ramjet," *5th Symposium (International) on Combustion*, The Combustion Inst., Pittsburgh, PA, 1955, pp. 48–56.

[14]Williams, F. A., "Flame Stabilization of Premixed Turbulent Gases," *Applied Mechanics Surveys*, edited by H. N. Abramson, H. Leibovitz, J. M. Crowley, and S. Juhasz, Spartan, Washington, DC, 1966, pp. 1157–1170.

[15]Ben-Arosh, R., and Gany, A., "Similarity and Scale Effects in Solid-Fuel Ramjet Combustors," *Journal of Propulsion and Power*, Vol. 8, No. 3, 1992, pp. 615–623.

[16]Netzer, D. W., "Modeling Solid Fuel Ramjet Combustion," *Journal of Spacecraft and Rockets*, Vol. 14, No. 12, 1977, pp. 762–766.

[17]Schulte, G., "Fuel Regression and Flame Stabilization Studies of Solid Fuel Ramjets," *Journal of Propulsion and Power*, Vol. 2, No. 4, 1986, pp. 301–304.

[18]"Solid Fuel Ramjet," United Technologies Chemical Systems, San Jose, CA.

[19]Roudakov, A. S., Schickhman, Y., Semenov, V., Novelli, P., and Fourt, O., "Flight Testing an Axisymmetric Scramjet—Russian Recent Advances," International Astronautical Federation, Paper 93-S.4.485, Oct. 1993.

[20]Zvuloni, R., Gany, A., and Levy, Y., "Geometric Effects on the Combustion in Solid Fuel Ramjets," *Journal of Propulsion and Power*, Vol. 5, No. 1, 1989, pp. 32–37.

[21]Hadar, I., and Gany, A., "Fuel Regression Mechanism in a Solid Fuel Ramjet," *Propellants, Explosives, Pyrotechnics*, Vol. 17, No. 3, 1992, pp. 70–76.